Journal of Colloid and Interface Science 532 (2018) 790–797

Contents lists available at ScienceDirect

Journal of Colloid and Interface Science

journal homepage: www.elsevier.com/locate/jcis

Regular Article

A carbon nanotube-embedded conjugated polymer mesh with controlled oil absorption and surface regeneration via *in situ* wettability switch

Jian Xu, Shichen Fu, Wei Xu, Eui-Hyeok Yang *

Stevens Institute of Technology, Mechanical Engineering Department, 1 Castle Point Terrace, Hoboken, NJ 07030, USA

GRAPHICAL ABSTRACT

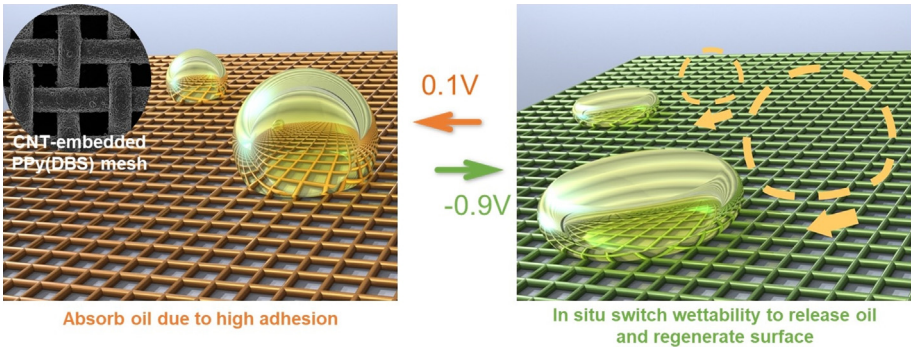

ARTICLE INFO

Article history:
Received 18 June 2018
Revised 13 August 2018
Accepted 13 August 2018
Available online 14 August 2018

Keywords:
Conjugated polymer
Surfactant
In situ wettability switch
Interfacial tension
Surface adhesion
Oil/water separation

ABSTRACT

This paper presents a mesh-type absorbent made of a carbon nanotube (CNT)-embedded polypyrrole dodecylbenzenesulfonate (PPy(DBS)) surface for controlled absorption and release of oils and regeneration of polymer surfaces toward continuous oil/water separation. The mesh absorbs dichloromethane (DCM) under oxidation in aqueous environment and releases them under reduction via *in situ* switching of underwater wettability. CNTs were grown out of stainless steel surfaces and embedded into the PPy (DBS) film, which enhanced the switchable wettability as well as the surface regeneration. The CNT-embedded morphology improved oil retention by a factor of two in an oxidized state and decreased wettability switch time by 16% in a reduced state over the mesh without CNT embedment during 250 redox cyclic testing. A rolled 2 cm × 3 cm CNT-embedded PPy(DBS) mesh was furthermore used to demonstrate the continuous absorption and release of oils, during which DCM of 16 times of the absorbent weight was collected in 50 redox cycles.

1. Introduction

There is an immense need for low-cost, efficient and reliable methods for oily water treatment and/or oil recovery. Recent decades, materials with special wetting properties and corresponding strategies have been developed for oil/water separation [1,2]. The oleophilic/hydrophobic or underwater oleophobic properties were utilized to separate water from water/oil mixture via absorption or filtration [2–4]. Materials with special wettability, including polymers [5,6,15,7–14], metals [7,16–23], carbon [24–28], silicon [5,14,15,22,29–34], or fluorine [5,11,19,23,34,35]-based compounds were fabricated on various substrates, such as meshes [8,9,35,10,12,15,18,22,27,28,31], fabric or textiles [5,7,14,16,20,21,30,33], sponges [6,29,32], foams [24,34], membranes [13,19,23,26], and aerogels [25], demonstrating oil/water

* Corresponding author.
E-mail address: eyang@stevens.edu (E.-H. Yang).

https://doi.org/10.1016/j.jcis.2018.08.041
0021-9797/

separation. The special wetting properties were further enhanced by incorporating macroscopic morphologies inherited from the substrates or microscopic structures via microfabrication using chemical etching [18,19,23,24,32,34], nanoparticles [7,10,14,16,17,29] or sol [20,30,31]. These structures enhanced the separation efficiency by introducing higher surface areas for oil absorption (Wenzel's model [36]) or entrapped air phase for oil rejection (Cassie–Baxter [37]).

While the synergistic effect of surface chemistry and structures enables the materials with special wetting, a strategy for the continuous operation would further enhance the efficiency of oil/water separation. For example, an uninterrupted filtration is possible using well-designed apparatus [7,11,15,17,18,31]. But, typically the oil absorbents gradually lose their wetting capability or reach the limit in absorbing capacity due to fouling or saturation. The degeneration of these materials warrants either the enhancement of their capacity via adding auxiliary receptacle such as bags [30,33] or skimmers [24], or the regeneration or cleaning of saturated materials via rinsing [6,9,30], squeezing [6,32], heating or burning [7,25], UV radiation [7,19,22], or pumping [29,30]. However, all these regeneration methods accompany the process down-time or require additional materials and labors. Various functional materials may enable continuous operation by allowing absorbed oil to be released 'on demand' using switching wettability via external stimuli such as temperature, pH, light, electrical, or magnetic field [38–44]. Materials with special wettability capable of *in situ* switching their wettability would enable controlled trap and release of oils toward continuous oil/water separation.

Here we demonstrate continuous absorption and release of dichloromethylene (DCM) via *in situ* switch of underwater wettability (*i.e.,* affinity for organic liquid in an aqueous environment) of a carbon nanotube (CNT)-embedded polypyrrole dodecylbenzenesulfonate (PPy(DBS)) mesh. We first grow CNTs on the stainless steel mesh surface, and subsequently electropolymerize PPy (DBS) atop CNTs. We oxidize or reduce PPy(DBS) meshes (with and without CNT embedment) in 0.1 M $NaNO_3$ to absorb and subsequently *in situ* release DCM, while simultaneously regenerating the polymer surface. We then prove that the CNT embedment enhances the surface wettability and longevity of the PPy(DBS) mesh. Lastly, we show a proof-of-concept oil collection and surface recovery of the polymer surface via *in situ* underwater wettability switch.

2. Working mechanism

Fig. 1 shows the mechanism of absorption of DCM and release of once-absorbed DCM using the PPy(DBS) mesh, and *in situ* regeneration of the PPy(DBS) surface (*i.e.,* regeneration without moving the mesh out of electrolyte or using any additional material to the system). PPy(DBS) switches its underwater wettability *in situ* upon application of voltages as low as ±1 V [45–47]. When a positive voltage (e.g., 0.1 V) is applied, PPy(DBS) surface is oxidized with a strong adhesion toward oils (therefore the PPy(DBS) mesh can 'absorb' oils by adhering the oils on the PPy(DBS) surface (Fig. 1a-i, ii). When a negative voltage (e.g., −0.9 V) is applied, the PPy(DBS) surface is reduced, where previously attached oil droplets roll off from the mesh (Fig. 1b-i) or permeate through the mesh (Fig. 1b-ii). This switching of underwater wettability, as has been previously reported [46–48], is attributed to the reorientation and desorption of DBS^- molecules [49,50]. Being amphiphilic,

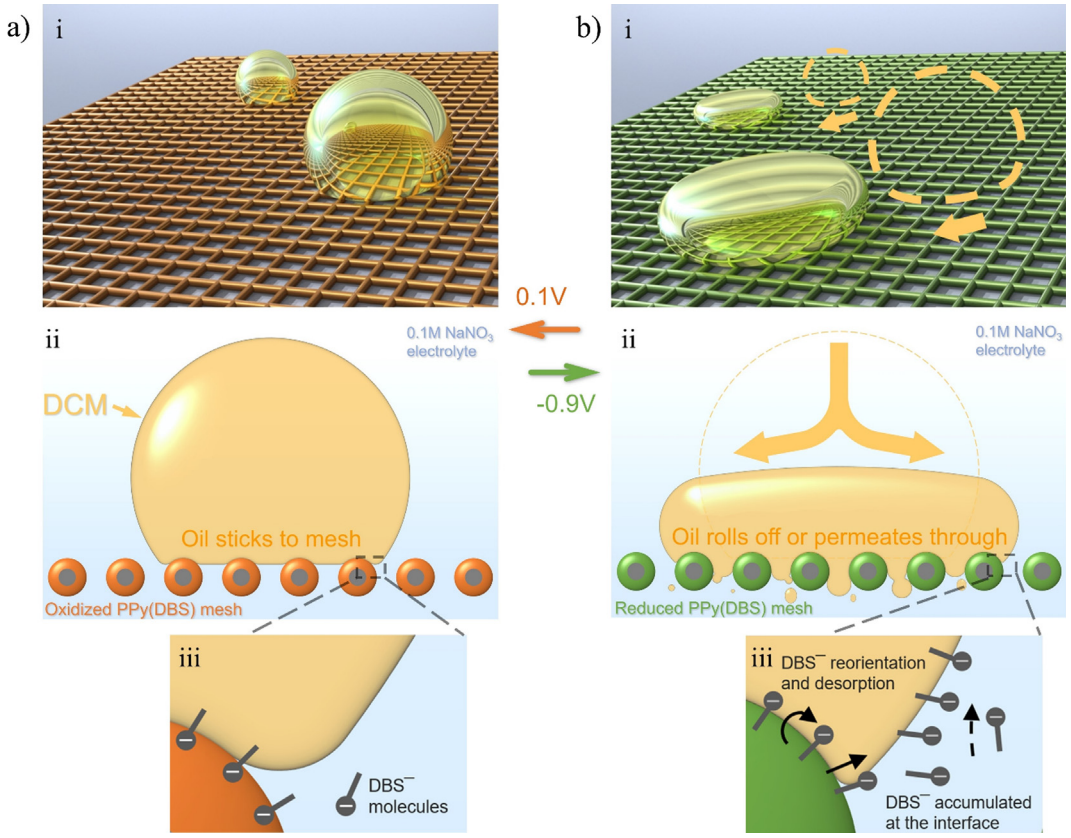

Fig. 1. Schematic illustration of the mechanism of oil absorption and release using a PPy(DBS) mesh via *in situ* wettability switch. (a) Oxidized PPy(DBS) surface shows strong affinity to oils [49], adhering the oils on the polymer surface. Therefore, the PPy(DBS) mesh can be used to 'absorb' oils. (b) Upon reduction, PPy(DBS) surface *in situ* switches underwater wettability, allowing oils to be released from the mesh via rolling off or permeating through the pores (i, ii). This wettability switch is attributed to the reorientation and desorption of DBS^- molecules [49,50] (iii).

DBS^- molecules have hydrophobic (dodecyl chains) tails and hydrophilic (sulfonic acid group) heads. When PPy(DBS) is oxidized, DBS^- molecules bond to the polymer backbone via negative charged sulfonic acid group, leaving dodecyl chains protruding out and rendering surface underwater oleophilic (Fig. 1a-iii). When PPy(DBS) is reduced, DBS^- molecules either reorient, exposing their oleophobic heads, or desorb from the surface, accumulating at the oil/water interface (Fig. 1b-iii). This process makes surface oleophobic while reducing the interfacial tension. As a result, the retention force f (*i.e.*, the force needed to prevent oils from rolling off from the surface) decreases according to Furmidge equation [51–53]:

$$f = w\gamma(\cos\theta_R - \cos\theta_A) \quad (1)$$

where w is the droplet width, γ is the oil/water interfacial tension, and $\theta_{R,A}$ are the maximal advancing and minimal receding angles, respectively. Once the retention force is no longer balanced with gravitational or buoyant forces, the adhered oil rolls off from the mesh (Fig. 1b-i). Meanwhile, the breakthrough pressure, ΔP_B (*i.e.*, the hydrostatic pressure of oil droplets required to permeate through the pores of mesh) decreases as well according to Young-Laplace equation [54–56]:

$$\Delta P_B = \frac{2\gamma\cos\theta_A}{r} \quad (2)$$

where r is the pore radius. If the breakthrough pressure decreases to the point that can be overcome by the hydrostatic pressure of oil droplet, the oil permeates through pores of the mesh (Fig. 1b-ii).

We confirmed the desorption of DBS^- molecules from PPy(DBS) using energy-dispersive X-ray spectroscopy (EDS) and surface tension measurements [49]. Lateral actuation, and on-demand capture and release of oil droplets, have been demonstrated using this unique property [57,58]. Further studies also suggest the performance (e.g., switch time, longevity) of PPy(DBS) can be tuned by adjusting surface parameters (e.g., thickness, roughness, structure, morphology) [50,58,59].

3. Experiments

3.1. Fabrication

Multiwalled carbon nanotubes (CNTs) were directly grown from 304 stainless steel (SS) meshes (Size 200 × 200, McMaster-Carr, Robbinsville, NJ) using atmospheric pressure chemical vapor deposition (APCVD). SS meshes were cut, rinsed, dried and then placed in the center of a 2″ quartz tube in a horizontal three zone CVD furnace and heated to 750 °C under the flow of 60 sccm hydrogen (H_2, Praxair, Newark, NJ) and 500 sccm Argon (Ar, Praxair, Newark, NJ). Then, additional ethylene (C_2H_4, Praxair, Newark, NJ) were fed through the system at flow rates of 100 sccm for 7 mins for CNTs growth. Subsequently, the samples were rapidly cooled to room temperature by blowing air into the furnace.

After CNT growth, PPy(DBS) film was electropolymerized atop the CNT-covered SS mesh surface. First, 1 mL pyrrole monomer (reagent grade, 98%, Sigma-Aldrich, St. Louis, MO) was thoroughly mixed with 150 mL 0.1 mol/L sodium dodecylbenzenesulfonate (NaDBS, technical grade, Sigma-Aldrich, St. Louis, MO) solution. Then, CNT-covered SS mesh, a saturated calomel electrode (SCE, Fisher Scientific Inc., Pittsburgh, PA), and another SS mesh (5 cm × 5 cm) were submerged in the solution as the working, reference, and counter electrode, respectively. The coating of PPy(DBS) surfaces was carried out using a potentiostat (263A, Princeton Applied Research, Oak Ridge, TN) by applying 0.7 V to the working electrode (vs. SCE) and stopped once surface charge density reached 1 C/cm^2. The SS meshes deposited with 10 nm chromium (Cr) and 30 nm gold (Au) films using an e-beam evaporator (Explorer 14, Denton Vacuum, Moorestown, NJ), instead of CNTs, were also coated with PPy(DBS) surfaces using the same procedure. After fabrication, PPy(DBS) mesh surfaces were rinsed and dried in air overnight before any further characterizations.

3.2. Imaging

The surface morphologies of the SS mesh, before and after CNTs growth and PPy(DBS) polymerization were characterized using a scanning electron microscope (Auriga Small Dual-Beam FIB-SEM, Carl Zeiss, Jena, Germany) at 5 kV. The increase of PPy(DBS) surface area through the CNT embedment was examined by comparing surface profiles of CNT-embedded and those without CNTs using cross-section SEM images. Transmission electron microscopy (TEM) imaging of CNTs grown on SS mesh was also performed. For TEM imaging, a CNT-covered SS mesh was sonicated in ethanol to obtain a low-density, uniform solution of CNTs. A pipette was used to drop this solution on a lacey carbon TEM grid. High-magnification TEM images of CNTs were taken using a JEOL JEM2100F transmission electron microscope at 200 kV.

3.3. Wettability

The *in situ* switch of underwater wettability of PPy(DBS) was examined by analyzing the behavior of oil droplets on PPy(DBS) meshes in 0.1 mol/L $NaNO_3$ (*i.e.,* electrolyte). A schematic drawing of the experimental setup is shown in Fig. S1 in Supporting Material. First, PPy(DBS) was oxidized for 30 s, while the mesh was positioned horizontally and DCM droplets of various volumes were applied on the mesh. The mesh was then gradually tilted and positioned vertically to test the affinity of the PPy(DBS) to DCM droplets. Secondly, new DCM droplets were applied to slightly tilted (~1°) oxidized PPy(DBS) mesh, followed by reduction of PPy (DBS) until droplets roll off from the mesh. For both experiments, the whole process was recorded using a goniometer system (Model 250, Ramé-hart, Succasunna, NJ) and was repeated after different redox cycles. PPy(DBS) was oxidized/reduced at 0.1 V/−0.9 V versus a 13 mm × 35 mm platinum (Pt) mesh (*i.e.,* counter electrode). The wettability switch towards other oils (*i.e.*, hexane, cyclohexane, octane, nonane, dodecane, corn oil, and diesel oil) was also tested.

3.4. Absorption and release of DCM droplets

DCM dyed with methyl violet (Sigma-Aldrich, St. Louis, MO) was carefully dispensed into 0.1 mol/L $NaNO_3$ to form a distinguishable layer. The oxidized PPy(DBS) mesh was dipped in dyed DCM layer to absorb DCM and then was taken out of the DCM layer and reduced for 60 s to fully release DCM. PPy(DBS) surface was oxidized/reduced at 0.1 V/−0.9 V versus a 5 cm × 10 cm SS mesh (*i.e.,* counter electrode). To quantitatively show the amount of DCM transported by using the PPy(DBS) mesh, DCM was dispensed into a graduated vial submerged in $NaNO_3$ and transported to the other vial using PPy(DBS) mesh controlled by an axis stage. This demonstration process was fully recorded using a digital camera, and the experimental setup is shown in Fig. S2 in Supporting Material.

4. Results and discussion

4.1. Fabrication of CNT-embedded PPy(DBS) meshes

Fig. 2 shows the fabricated CNT-embedded PPy(DBS) meshes. After CNT growth, the SS mesh changed its color from original metallic silver (i) to dark grey (ii). SEM images show CNTs directly

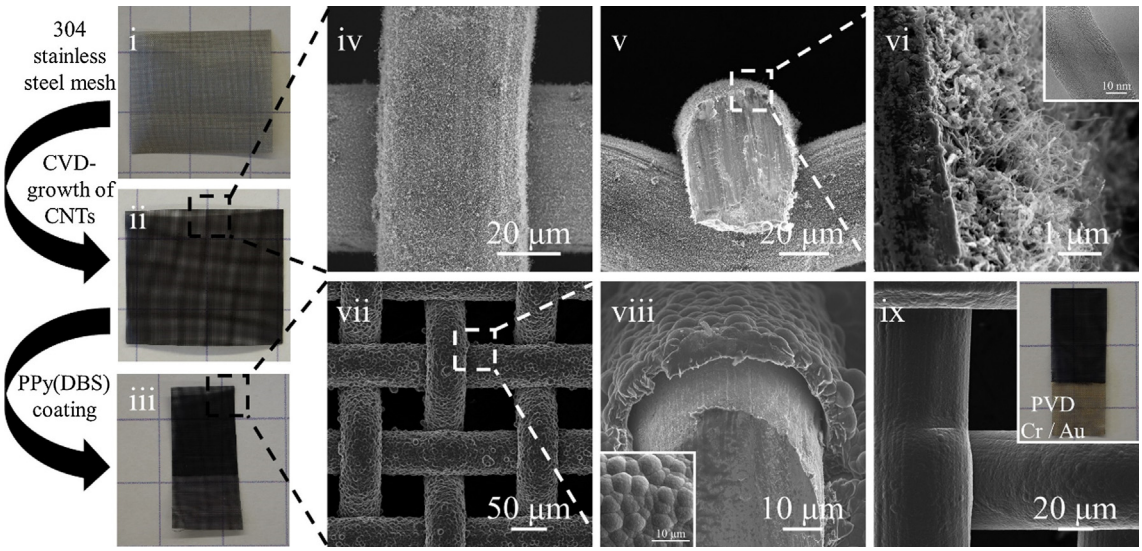

Fig. 2. Photo and SEM images of CNT-embedded PPy(DBS) meshes. On (i) 304 stainless steel (SS) mesh, (ii) CNTs were grown using CVD directly out of the SS surface, and (iii) PPy(DBS) was electropolymerized atop the CNT-grown SS surface. (iv–viii) SEM images of top and cross-sectional views of CNTs and CNT-embedded PPy(DBS) surfaces. Inset in (vi) shows TEM image of a CNT. The PPy(DBS) film was separated from the SS surface due to stress during the cutting of the mesh. (ix) PPy(DBS) without CNT embedment fabricated on Au-coated SS mesh, showing smooth morphology.

grown out of the SS surface (iv-vi). Top (iv) and cross-sectional (v, vi) views of the mesh after CNT growth further confirm that the CNTs thoroughly covered the whole surface of SS mesh. Fig. 2-vi shows the detailed images of CNTs with an average length of 2.5 μm and a diameter of 30 nm. The TEM image (inset in vi) shows the grown materials are multiwalled CNTs with the number of walls of approximately 20. Magnified and additional TEM images are shown in Fig. S3 in Supporting Material. CNTs significantly enhanced the conductivity of the original SS mesh surfaces, allowing more uniform and efficient electropolymerization of PPy (DBS). In comparison, PPy(DBS) electropolymerized on a mesh without CNTs is shown in Fig. S4 in Supporting Material, which depicts a less uniform coating of PPy(DBS) than the PPy(DBS) electropolymerized on the CNT-grown SS surface.

After electropolymerization of PPy(DBS) on CNT-covered SS mesh, the color of mesh became darker while less gloss (iii). SEM images in Fig. 2-vii, viii show the CNT-embedded morphology formed after the electropolymerization of PPy(DBS) atop the CNT-grown SS surface. The magnified cross-sectional view of CNT-embedded polymer mesh (viii) confirms that the thickness of PPy(DBS) film is approximately 8 μm, agreeing with the PPy (DBS) surfaces grown on flat substrates in our previous report [50]. Compared to the PPy(DBS) surfaces fabricated on SS meshes coated with Au (*i.e.,* without CNTs) (ix), PPy(DBS) surfaces electropolymerized on CNT-covered SS had nodules with an average size of 7 μm over the whole surface. This morphology increased the surface area of PPy(DBS) by 30%, which resulted in the enhancement of surface wettability (discussed in next section).

4.2. Absorption and release of DCM

After fabricating PPy(DBS) meshes, we demonstrate controlled absorption and release of DCM. First, an oxidized PPy(DBS) mesh (in $NaNO_3$ electrolyte) was dipped in and out of DCM (dyed with purple) as depicted in Fig. 3a–c, where the mesh absorbed DCM, owing to the strong adhesion of DCM to the oxidized PPy(DBS) surface. As shown Fig. 3a and c, the color of PPy(DBS) mesh turned from original dark grey to purple, indicating a successful absorption of DCM. Then, the mesh was moved to a new location within electrolyte without losing DCM, followed by PPy(DBS) reduction.

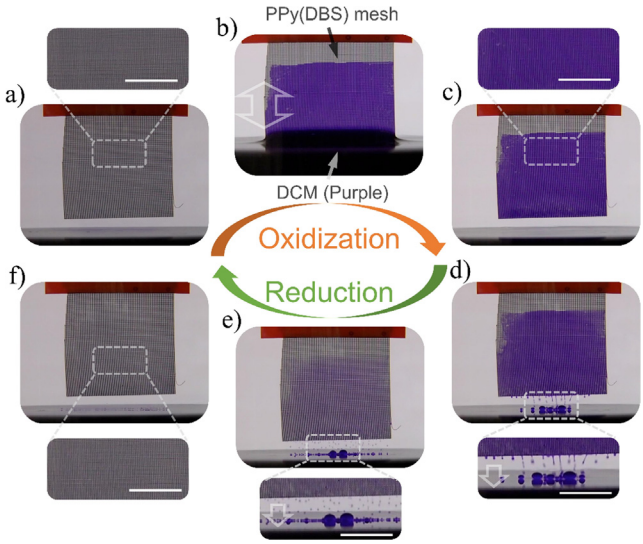

Fig. 3. Absorption and release of DCM using a PPy(DBS) mesh, and *in situ* regeneration of PPy(DBS) surface. (a) An unused oxidized PPy(DBS) mesh (dark grey). (b) PPy(DBS) mesh was dipped in and out of DCM dyed in purple. (c) The color of PPy(DBS) turned purple, indicating it successfully absorbed DCM. (d) Upon reduction, DCM was released from the mesh via *in situ* switch of surface wettability. (e) DCM continued to be released. (f) After 60 s of reduction, DCM was fully released from the mesh (dark grey). The mesh was regenerated for the next cycle of oil absorption and release. Mesh size is 1.75 × 2.1 cm. The scale bars in insets are 0.5 cm. (For interpretation of the references to color in this figure legend, the reader is referred to the web version of this article.)

During reduction (Fig. 3d–f), the PPy(DBS) surface *in situ* switched its wettability, allowing DCM to be fully released from the mesh. After reduction for 60 s, the color of PPy(DBS) mesh turned back to dark grey (Fig. 3f), suggesting that the once absorbed DCM droplets were fully released from the mesh. While the DCM was released, the PPy(DBS) surface was simultaneously *in situ* regenerated (*i.e.,* the surface was regenerated without moving the mesh out of electrolyte or using any additional material to the system). After completing this oil absorption and release cycle with simultaneous regeneration of the PPy(DBS) surface, the PPy(DBS) mesh was oxidized again, ready for another cycle of absorption and

release (*i.e.,* consecutive process). Together, this process demonstrates the continuous absorption and release of oils, while regenerating the PPy(DBS) surface via *in situ* wettability switch. A video recording, which shows the absorption and release of DCM using a PPy(DBS) mesh, is included in Supporting Material as Video S1.

4.3. Effects of CNT-embedded morphology

Fig. 4 shows *in situ* switch of underwater wettability of PPy (DBS) towards oils and the effects of the CNT embedment. Fig. 4a shows a DCM droplet with a contact angle of 125° on a horizontally positioned oxidized PPy(DBS) mesh. The droplet was pinned on the vertically positioned mesh, indicating strong adhesion of DCM on the oxidized PPy(DBS) surface. For DCM droplets with a volume of 4 μL, this strong affinity of the CNT-embedded PPy(DBS) mesh to DCM was maintained during 250 redox cycles (test was voluntarily stopped after 250 cycles). In contrast, the DCM roll-off angle was gradually decreased to 84°, 71°, 58°, and 56° on the PPy(DBS) mesh without CNTs after 100, 150, 200, and 250 redox cycles, respectively (Fig. 4b). In addition, we found the roll-off angle also depends on the droplet volume. For example, DCM droplets with volumes of 2.9 μL, 3.5 μL, and 5.0 μL rolled off at tilting angles of 83°, 80°, and 28°, respectively, on oxidized PPy(DBS) meshes without CNTs after 100 redox cycles. Therefore, we further used the retention force to study the oil trapping capability of oxidized PPy(DBS) mesh, which is calculated as

$$f = (\rho_o - \rho_w)Vg\sin\alpha \quad (3)$$

where ρ_o and ρ_w are the densities of oil (DCM) and water (0.1 M $NaNO_3$), V is the volume of the DCM droplets, g is the gravitational acceleration and α is the roll-off angles of the DCM droplets (<90°) [52]. The retention forces were measured for PPy(DBS) meshes both with and without CNT embedment after multiple redox cycles, each using at least 3 droplets with different volumes with roll-off angles smaller than 90°. The measured maximum retention forces are shown in Fig. 4c. While the PPy(DBS) mesh without CNTs showed the retention force of 21.4 mN, 11.1 mN, and 7.1 mN after 0, 100, and 250 redox cycles, the CNT-embedded PPy(DBS) mesh showed the retention force of 25.7 mN, 20.6 mN, and 16.9 mN, which were measured after 0, 100, and 250 redox cycles. These results show an enhancement of 19.8%, 85.5%, and 137.9%, respectively, over the results using the mesh without CNTs. In addition, CNT-embedded PPy(DBS) mesh demonstrated a slower loss of retention force (*i.e.,* 34.1% decrease compared to 66.7% decrease for the mesh without CNTs after 250 redox cycles). The loss of retention force is generally attributed to the loss of oleophilicity of oxidized PPy(DBS) surface, the influx of hydronium from the electrolyte into the polymer, or the accumulation of surfactant dopants on the surface [46,60–62]. However, CNT-embedded PPy(DBS) surface enhanced the surface oleophilicity, given higher roll-off angles and stronger retention force throughout 250 redox cycles. We attribute the enhanced surface oleophilicity to the embedded CNTs, which increases surface area and roughness; hence, there exists more surface area for oil droplets to contact with oxidized PPy(DBS) surface, resulting in stronger adhesion between the surface and the oil.

When PPy(DBS) is reduced, it switches wettability *in situ,* allowing the previously absorbed droplet to roll off from or permeate

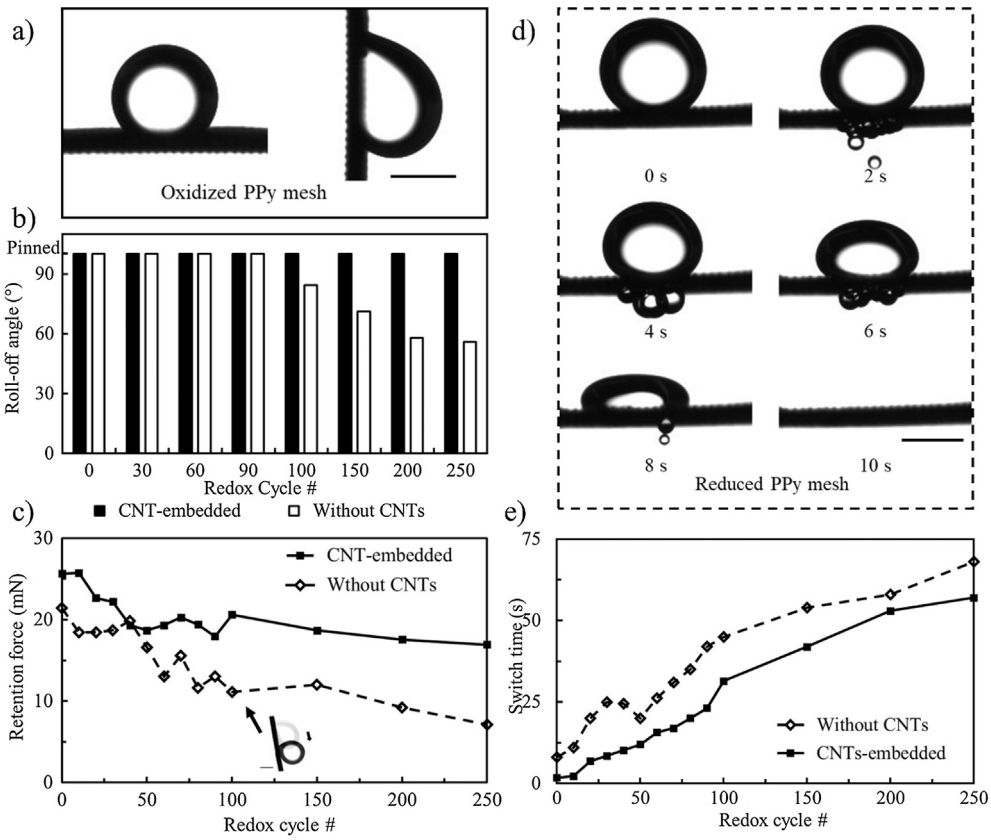

Fig. 4. Tunable wettability of PPy(DBS) mesh and enhancement of retention force and switch time due to the CNT embedment. (a) DCM droplet (2.1 μL) on an oxidized PPy (DBS) mesh (CNT-embedded, 0 redox cycle). (b) Roll-off angles of 4 μL DCM droplets on an oxidized PPy(DBS) mesh after multiple redox cycles. (c) Retention forces of an oxidized PPy(DBS) mesh after multiple redox cycles. The calculated maximum retention force by the PPy(DBS) mesh without CNTs after 100 redox cycles was 11.1 mN, corresponding to a 3.5 μL DCM droplet rolled off at 80° as shown in the inset. (d) DCM droplets (3 μL) rolled off from or permeated through PPy(DBS) mesh (without CNTs, 0 redox cycle) during reduction. (e) Switch time of PPy(DBS) mesh after multiple redox cycles. Switch time is marked as the reduction time required for the droplet to start rolling off. Scale bar is 1 mm.

through the mesh. Fig. 4d shows that a DCM droplet starts permeating through the pores of the reduced PPy(DBS) mesh in less than 2 s. The DCM droplet was fully removed from the mesh after 10 s of reduction. Other oils were also tested, demonstrating similar roll off behaviors during reduction as shown in Fig. S5 in Supporting Material. Fig. 4e shows the change in 'switch time', (*i.e.,* the time required for DCM droplets to start rolling off from a PPy(DBS) mesh once it is reduced) with the redox cycles. The switch times for the mesh without CNTs were 8, 45, and 68 s after 0, 100, and 250 redox cycles, respectively. In contrast, the switch times for the CNT-embedded mesh were 1.8, 31.4, and 57 s, respectively. The gradual increase of switch time after redox cycles is due to the loss of DBS^- molecules from polymer surface after each reduction. However, CNT-embedded morphology shortens the switch time, because it provides a higher surface area, which increases the amount of DBS^- molecules desorbed from PPy(DBS) surfaces under reduction, facilitating more rapid decrease of oil/water interfacial tension and retention force [58,59].

4.4. Continuous DCM transport and surface regeneration

PPy(DBS) meshes were used to demonstrate the absorption and transport of DCM in 0.1 M $NaNO_3$ environment from one vial to another, and to show the release of DCM droplets from the mesh while simultaneously regenerating PPy(DBS) surfaces, as the first step toward continuous oil/water separation. The experiment was performed using the setup shown in Fig. 5a. First, a 2 cm × 3 cm PPy(DBS) mesh surface was rolled up, oxidized and dipped in and out of the left vial filled with DCM (dyed in purple). Owing to the strong adhesion towards oil, DCM was absorbed on the mesh and transferred to the right vial. PPy(DBS) surfaces were then reduced, allowing DCM attached to the PPy(DBS) surfaces to be released and reclaimed into the right vial, while simultaneously regenerating the PPy(DBS) surface. This process of DCM absorption, transport and release was repeated for 50 cycles as shown in Fig. 5b. After 50 continuous redox cycles (see Fig. 5c), 2.2 mL of DCM was moved using PPy(DBS) mesh without CNTs, which was 11 times of the weight of the entire mesh. In contrast, 3.1 mL of DCM was collected using CNT-embedded mesh, 16 times of its weight. The enhanced DCM collection is attributed to the additional surface area and stronger retention force as described earlier. In addition, the DCM transfer rate was nearly linear as depicted in Fig. 5c, indicating that the amount of DCM transferred during each cycle was nearly identical. This suggests that the adhesion between oxidized PPy(DBS) surface and DCM is still strong enough to maintain the absorption capacity, though retention force slightly decreases after redox cycles (Fig. 4b, c).

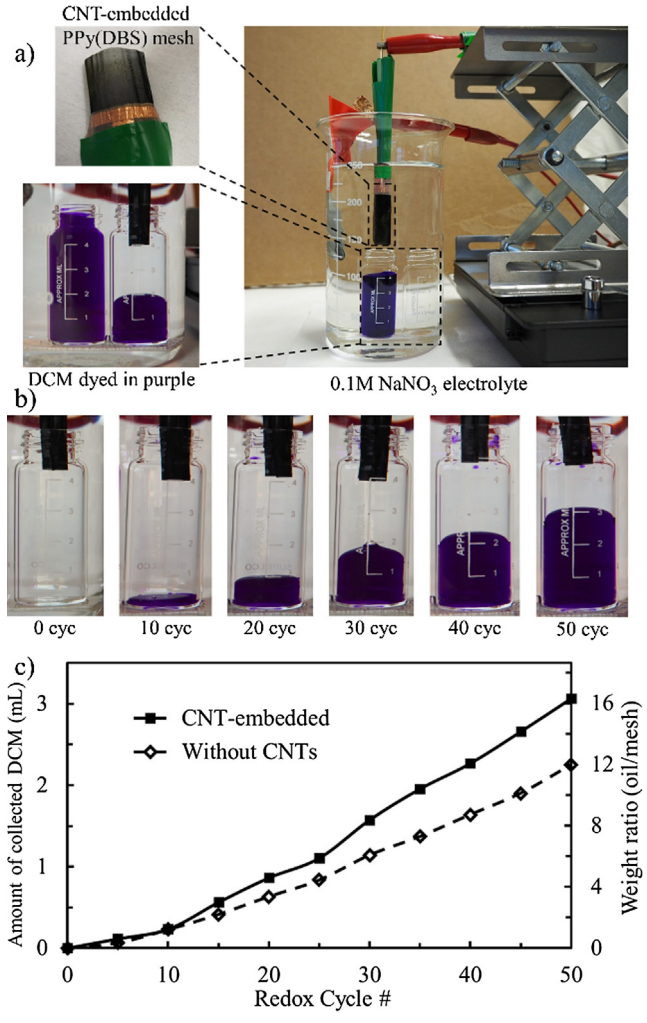

Fig. 5. Absorption, transport and release of DCM using a PPy(DBS) mesh. (a) Oil collection setup with the PPy(DBS) mesh. (b) DCM transport for 50 continuous redox cycles using CNT-embedded PPy(DBS) mesh. (c) Amount of DCM collected using the PPy(DBS) mesh (2 cm × 3 cm) with and without CNT embedment after 50 redox cycles. Second y axis shows the weight ratio between the transported DCM and the PPy(DBS) mesh.

5. Conclusion

While numerous mesh-based materials have been developed and used for oil/water separation, one requires special considerations for highly efficient and continuous process. These considerations include integration of both superhydrophobic and superhydrophilic materials [63], use of Janus gradient materials [64], or switching of materials' wettability using external stimuli such as magnetic field [65], temperature, pH, UV radiation [22,66], vapor exposure [67], electrical signals [68], or their combinations [69–71]. This paper reports on the switch of surface wettability achieved via decrease of oil/water interfacial tension during electrochemical redox of PPy(DBS). The advantages of this method include *in situ* wettability switch, relatively short switch time (within seconds), low operation voltage (±1 V), and good cyclability (e.g., performance maintained in 250 tested cycles). We have utilized *in situ* wettability switch of PPy(DBS) surfaces, and demonstrated the controlled absorption, transport, and release of oils using a CNT-embedded PPy(DBS) mesh. The mesh with oxidized PPy(DBS) was used to absorb oils owing to its high affinity to oils, and the mesh with reduced PPy(DBS) was used to release the oils via switching its oil affinity, while simultaneously regenerating the polymer surface. In addition, we embedded CNTs into the PPy(DBS) film to enhance the efficiency of wettability switch. CNT-embedded PPy(DBS) meshes showed 138% higher retention force and 16% shorter switch time after 250 redox cycles than PPy(DBS) meshes without CNTs. The CNT-embedded PPy(DBS) mesh was then used to demonstrate a continuous absorption and transport of DCM, collecting 16 times heavier DCM than the weight of the mesh in 50 redox cycles. Further study is underway to elucidate the functionality of PPy(DBS) surfaces for other common organic pollutants, and to increase the absorption capacity for highly efficient, continuous and automatic oil/water separation.

Acknowledgement

This work has been supported in part by National Science Foundation awards (Grants ECCS-1202269 and EEC-1138244) and the Defense University Research Instrumentation Program (Grant FA9550-11-1-0272). Acknowledgment is also made to the donors

of the American Chemical Society Petroleum Research Fund for partial support of this research. This work has also been partially carried out at the Micro Device Laboratory (MDL), the Laboratories for Multiscale Imaging (LMSI) at Stevens Institute of Technology, and the Center for Functional Nanomaterials (CFN) at Brookhaven National Laboratory under Contract No. DE-SC0012704. The authors thank Dr. Tseng-Ming Chou (LMSI) and Dr. Lihua Zhang (CFN) for their assistance for TEM characterization.

Appendix A. Supplementary material

Supplementary data associated with this article can be found, in the online version, at https://doi.org/10.1016/j.jcis.2018.08.041.

References

[1] R.P. Schwarzenbach, T. Egli, T.B. Hofstetter, U. von Gunten, B. Wehrli, Global water pollution and human health, Annu. Rev. Environ. Resour. 35 (2010) 109–136, https://doi.org/10.1146/annurev-environ-100809-125342.
[2] Z. Chu, Y. Feng, S. Seeger, Oil/water separation with selective superantiwetting/superwetting surface materials, Angew. Chem. – Int. Ed. 54 (2015) 2328–2338, https://doi.org/10.1002/anie.201405785.
[3] Q. Ma, H. Cheng, A.G. Fane, R. Wang, H. Zhang, Recent development of advanced materials with special wettability for selective oil/water separation, Small 12 (2016) 2186–2202, https://doi.org/10.1002/smll.201503685.
[4] J. Ge, H. Zhao, H. Zhu, J. Huang, L. Shi, S. Yu, Advanced sorbents for oil-spill cleanup: recent advances and future perspectives, Adv. Mater. 28 (2016) 10459–10490, https://doi.org/10.1002/adma.201601812.
[5] X. Zhou, Z. Zhang, X. Xu, F. Guo, X. Zhu, X. Men, B. Ge, Robust and durable superhydrophobic cotton fabrics for oil/water separation, ACS Appl. Mater. Interfaces 5 (2013) 7208–7214, https://doi.org/10.1021/am4015346.
[6] X. Zhou, Z. Zhang, X. Xu, X. Men, X. Zhu, Facile fabrication of superhydrophobic sponge with selective absorption and collection of oil from water, Ind. Eng. Chem. Res. 52 (2013) 9411–9416, https://doi.org/10.1021/ie400942t.
[7] W. Zhang, X. Lu, Z. Xin, C. Zhou, A self-cleaning polybenzoxazine/TiO_2 surface with superhydrophobicity and superoleophilicity for oil/water separation, Nanoscale 7 (2015) 19476–19483, https://doi.org/10.1039/C5NR06425B.
[8] M. Liu, J. Li, L. Shi, Z. Guo, H.Q. Tang, H.X. Sun, B.P. Yang, A. Li, L. Jiang, Y.Q. Wen, X.J. Zhang, S.T. Wang, Stable underwater superoleophobic conductive polymer coated meshes for high-efficiency oil–water separation, RSC Adv. 5 (2015) 33077–33082, https://doi.org/10.1039/C5RA01681A.
[9] P.S. Brown, O.D.L.A. Atkinson, J.P.S. Badyal, Ultrafast oleophobic-hydrophilic switching surfaces for antifogging, self-cleaning, and oil-water separation, ACS Appl. Mater. Interfaces 6 (2014) 7504–7511, https://doi.org/10.1021/am500882y.
[10] P.S. Brown, B. Bhushan, Mechanically durable, superoleophobic coatings prepared by layer-by-layer technique for anti-smudge and oil-water separation, Sci. Rep. 5 (2015) 1–9, https://doi.org/10.1038/srep08701.
[11] A.K. Kota, G. Kwon, W. Choi, J.M. Mabry, A. Tuteja, Hygro-responsive membranes for effective oil–water separation, Nat. Commun. 3 (2012) 1025, https://doi.org/10.1038/ncomms2027.
[12] Z. Xue, S. Wang, L. Lin, L. Chen, M. Liu, L. Feng, L. Jiang, A novel superhydrophilic and underwater superoleophobic hydrogel-coated mesh for oil/water separation, Adv. Mater. 23 (2011) 4270–4273, https://doi.org/10.1002/adma.201102616.
[13] G. Kwon, A.K. Kota, Y. Li, A. Sohani, J.M. Mabry, A. Tuteja, On-demand separation of oil-water mixtures, Adv. Mater. 24 (2012) 3666–3671, https://doi.org/10.1002/adma.201201364.
[14] L. Zhang, Z. Zhang, P. Wang, Smart surfaces with switchable superoleophilicity and superoleophobicity in aqueous media: toward controllable oil/water separation, NPG Asia Mater. 4 (2012) e8, https://doi.org/10.1038/am.2012.14.
[15] M. Cao, X. Luo, H. Ren, J. Feng, Hot water-repellent and mechanically durable superhydrophobic mesh for oil/water separation, J. Colloid Interface Sci. 512 (2018) 567–574, https://doi.org/10.1016/j.jcis.2017.10.059.
[16] J.Y. Huang, S.H. Li, M.Z. Ge, L.N. Wang, T.L. Xing, G.Q. Chen, X.F. Liu, S.S. Al-Deyab, K.Q. Zhang, T. Chen, Y.K. Lai, Robust superhydrophobic TiO_2 @fabrics for UV shielding, self-cleaning and oil–water separation, J. Mater. Chem. A 3 (2015) 2825–2832, https://doi.org/10.1039/C4TA05332J.
[17] A.K. Sasmal, C. Mondal, A.K. Sinha, S.S. Gauri, J. Pal, T. Aditya, M. Ganguly, S. Dey, T. Pal, Fabrication of superhydrophobic copper surface on various substrates for roll-off, self-cleaning, and water/oil separation, ACS Appl. Mater. Interfaces 6 (2014) 22034–22043, https://doi.org/10.1021/am5072892.
[18] F. Zhang, W. Bin Zhang, Z. Shi, D. Wang, J. Jin, L. Jiang, Nanowire-haired inorganic membranes with superhydrophilicity and underwater ultralow adhesive superoleophobicity for high-efficiency oil/water separation, Adv. Mater. 25 (2013) 4192–4198, https://doi.org/10.1002/adma.201301480.
[19] L. Li, Z. Liu, Q. Zhang, C. Meng, T. Zhang, J. Zhai, Underwater superoleophobic porous membrane based on hierarchical TiO_2 nanotubes: multifunctional integration of oil–water separation, flow-through photocatalysis and self-cleaning, J. Mater. Chem. A 3 (2015) 1279–1286, https://doi.org/10.1039/C4TA04699D.
[20] X. Zheng, Z. Guo, D. Tian, X. Zhang, W. Li, L. Jiang, Underwater self-cleaning scaly fabric membrane for oily water separation, ACS Appl. Mater. Interfaces 7 (2015) 4336–4343, https://doi.org/10.1021/am508814g.
[21] S. Li, J. Huang, M. Ge, C. Cao, S. Deng, S. Zhang, G. Chen, K. Zhang, S.S. Al-Deyab, Y. Lai, Robust flower-like TiO_2@cotton fabrics with special wettability for effective self-cleaning and versatile oil/water separation, Adv. Mater. Interfaces 2 (2015) 1–11, https://doi.org/10.1002/admi.201500220.
[22] L. Zhang, Y. Zhong, D. Cha, P. Wang, A self-cleaning underwater superoleophobic mesh for oil-water separation, Sci. Rep. 3 (2013) 2326, https://doi.org/10.1038/srep02326.
[23] Y.-K. Lai, Y.-X. Tang, J.-Y. Huang, F. Pan, Z. Chen, K.-Q. Zhang, H. Fuchs, L.-F. Chi, Bioinspired TiO_2 nanostructure films with special wettability and adhesion for droplets manipulation and patterning, Sci. Rep. 3 (2013) 3009, https://doi.org/10.1038/srep03009.
[24] J. Song, Y. Lu, J. Luo, S. Huang, L. Wang, W. Xu, I.P. Parkin, Barrel-shaped oil skimmer designed for collection of oil from spills, Adv. Mater. Interfaces 2 (2015) 1500350, https://doi.org/10.1002/admi.201500350.
[25] Z.-Y. Wu, C. Li, H.-W. Liang, Y.-N. Zhang, X. Wang, J.-F. Chen, S.-H. Yu, Carbon nanofiber aerogels for emergent cleanup of oil spillage and chemical leakage under harsh conditions, Sci. Rep. 4 (2014) 4079, https://doi.org/10.1038/srep04079.
[26] C. Lee, S. Baik, Vertically-aligned carbon nano-tube membrane filters with superhydrophobicity and superoleophilicity, Carbon N. Y. 48 (2010) 2192–2197, https://doi.org/10.1016/j.carbon.2010.02.020.
[27] J. Chen, K. Li, H. Zhang, J. Liu, S. Wu, Q. Fan, H. Xue, Highly efficient and robust oil/water separation materials based on wire mesh coated by reduced graphene oxide, Langmuir 33 (2017) 9590–9597, https://doi.org/10.1021/acs.langmuir.7b01856.
[28] Y.Q. Liu, Y.L. Zhang, X.Y. Fu, H.B. Sun, Bioinspired underwater superoleophobic membrane based on a graphene oxide coated wire mesh for efficient oil/water separation, ACS Appl. Mater. Interfaces 7 (2015) 20930–20936, https://doi.org/10.1021/acsami.5b06326.
[29] J. Ge, Y. Ye, H. Yao, X. Zhu, X. Wang, L. Wu, J. Wang, H. Ding, N. Yong, L. He, S. Yu, Pumping through porous hydrophobic/oleophilic materials: an alternative technology for oil spill remediation, Angew. Chemie Int. Ed. 53 (2014) 3612–3616, https://doi.org/10.1002/anie.201310151.
[30] C. Cao, M. Ge, J. Huang, S. Li, S. Deng, S. Zhang, Z. Chen, K. Zhang, S.S. Al-Deyab, Y. Lai, Robust fluorine-free superhydrophobic PDMS–ormosil@fabrics for highly effective self-cleaning and efficient oil–water separation, J. Mater. Chem. A 4 (2016) 12179–12187, https://doi.org/10.1039/C6TA04420D.
[31] C.R. Crick, J.A. Gibbins, I.P. Parkin, Superhydrophobic polymer-coated copper-mesh; membranes for highly efficient oil–water separation, J. Mater. Chem. A 1 (2013) 5943, https://doi.org/10.1039/c3ta10636e.
[32] Q. Zhu, Y. Chu, Z. Wang, N. Chen, L. Lin, F. Liu, Q. Pan, Robust superhydrophobic polyurethane sponge as a highly reusable oil-absorption material, J. Mater. Chem. A 1 (2013) 5386–5393, https://doi.org/10.1039/c3ta00125c.
[33] J. Zhang, S. Seeger, Polyester materials with superwetting silicone nanofilaments for oil/water separation and selective oil absorption, Adv. Funct. Mater. 21 (2011) 4699–4704, https://doi.org/10.1002/adfm.201101090.
[34] X. Zhang, Z. Li, K. Liu, L. Jiang, Bioinspired multifunctional foam with self-cleaning and oil/water separation, Adv. Funct. Mater. 23 (2013) 2881–2886, https://doi.org/10.1002/adfm.201202662.
[35] I.S. Bayer, M.K. Tiwari, C.M. Megaridis, Biocompatible poly(vinylidene fluoride)/cyanoacrylate composite coatings with tunable hydrophobicity and bonding strength, Appl. Phys. Lett. 93 (2008), https://doi.org/10.1063/1.3009292 173902.
[36] R.N. Wenzel, Resistance of solid surfaces to wetting by water, Ind. Eng. Chem. 28 (1936) 988–994.
[37] A.B.D. Cassie, S. Baxter, Wettability of porous surfaces, Trans. Faraday Soc. 40 (1944) 546–551, https://doi.org/10.1039/tf9444000546.
[38] M. Liu, L. Jiang, Switchable adhesion on liquid/solid interfaces, Adv. Funct. Mater. 20 (2010) 3753–3764, https://doi.org/10.1002/adfm.201001208.
[39] J. Isaksson, C. Tengstedt, M. Fahlman, N.D. Robinson, M. Berggren, A Solid-state organic electronic wettability switch, Adv. Mater. 16 (2004) 316–320, https://doi.org/10.1002/adma.200306131.
[40] Z. Cheng, L. Feng, L. Jiang, Tunable adhesive superhydrophobic surfaces for superparamagnetic microdroplets, Adv. Funct. Mater. 18 (2008) 3219–3225, https://doi.org/10.1002/adfm.200800481.
[41] J. Yuan, X. Liu, O. Akbulut, J. Hu, S.L. Suib, J. Kong, F. Stellacci, Superwetting nanowire membranes for selective absorption, Nat. Nanotechnol. 3 (2008) 332–336, https://doi.org/10.1038/nnano.2008.136.
[42] C. Li, R. Guo, X. Jiang, S. Hu, L. Li, X. Cao, H. Yang, Y. Song, Y. Ma, L. Jiang, Reversible switching of water-droplet mobility on a superhydrophobic surface based on a phase transition of a side-chain liquid-crystal polymer, Adv. Mater. 21 (2009) 4254–4258, https://doi.org/10.1002/adma.200900903.
[43] K. Ichimura, S.-K. Oh, M. Nakagawa, Light-driven motion of liquids on a photoresponsive surface, Science (80-.) 288 (2000) 1624–1626, https://doi.org/10.1126/science.288.5471.1624.
[44] C. Li, Y. Zhang, J. Ju, F. Cheng, M. Liu, L. Jiang, Y. Yu, In situ fully light-driven switching of superhydrophobic adhesion, Adv. Funct. Mater. 22 (2012) 760–763, https://doi.org/10.1002/adfm.201101922.
[45] Y.-T. Tsai, C.-H. Choi, N. Gao, E.H. Yang, Tunable wetting mechanism of polypyrrole surfaces and low-voltage droplet manipulation via redox, Langmuir 27 (2011) 4249–4256, https://doi.org/10.1021/la104403w.

[46] M. Liu, F.-Q. Nie, Z. Wei, Y. Song, L. Jiang, In situ electrochemical switching of wetting state of oil droplet on conducting polymer films, Langmuir 26 (2010) 3993–3997, https://doi.org/10.1021/la903392n.
[47] J.A. Halldorsson, S.J. Little, D. Diamond, G.M. Spinks, G.G. Wallace, Controlled transport of droplets using conducting polymers, Langmuir 25 (2009) 11137–11141, https://doi.org/10.1021/la900835w.
[48] G. Chatzipirpiridis, A. Sanoria, O. Ergeneman, J. Sort, J. Puigmartí-Luis, B.J. Nelson, E. Pellicer, S. Pané, The electrochemical manipulation of apolar solvent drops in aqueous electrolytes by altering the surface polarity of polypyrrole architectures, Electrochem. Commun. 54 (2015) 32–35, https://doi.org/10.1016/j.elecom.2015.02.014.
[49] W. Xu, J. Xu, C.-H. Choi, E.H. Yang, In situ control of underwater-pinning of organic droplets on a surfactant-doped conjugated polymer surface, ACS Appl. Mater. Interfaces 7 (2015) 25608–25617, https://doi.org/10.1021/acsami.5b07589.
[50] J. Xu, A. Palumbo, W. Xu, E.H. Yang, Effects of electropolymerization parameters of PPy(DBS) surfaces on the droplet flattening behaviors during redox, J. Phys. Chem. B 120 (2016) 10381–10386, https://doi.org/10.1021/acs.jpcb.6b05698.
[51] C.G. Furmidge, Studies at phase interfaces. I. The sliding of liquid drops on solid surfaces and a theory for spray retention, J. Colloid Sci. 17 (1962) 309–324, https://doi.org/10.1016/0095-8522(62)90011-9.
[52] R. Tadmor, K. Chaurasia, P.S. Yadav, A. Leh, P. Bahadur, L. Dang, W.R. Hoffer, Drop retention force as a function of resting time, Langmuir 24 (2008) 9370–9374, https://doi.org/10.1021/la7040696.
[53] R. Tadmor, Approaches in wetting phenomena, Soft Matter. 7 (2011) 1577–1580, https://doi.org/10.1039/c0sm00775g.
[54] D. Tian, X. Zhang, X. Wang, J. Zhai, L. Jiang, Micro/nanoscale hierarchical structured ZnO mesh film for separation of water and oil, Phys. Chem. Chem. Phys. 13 (2011) 14606–14610, https://doi.org/10.1039/c1cp20671k.
[55] B.R. Solomon, M.N. Hyder, K.K. Varanasi, Separating oil-water nanoemulsions using flux-enhanced hierarchical membranes, Sci. Rep. 4 (2014) 1–6, https://doi.org/10.1038/srep05504.
[56] C. Zeiger, J. Kumberg, F. Vüllers, M. Worgull, H. Hölscher, M.N. Kavalenka, Selective filtration of oil/water mixtures with bioinspired porous membranes, RSC Adv. 7 (2017) 32806–32811, https://doi.org/10.1039/c7ra05385a.
[57] W. Xu, J. Xu, X. Li, Y. Tian, C.-H. Choi, E.H. Yang, Lateral actuation of an organic droplet on conjugated polymer electrodes via imbalanced interfacial tensions, Soft Matter. 12 (2016) 6902–6909, https://doi.org/10.1039/C6SM01223J.
[58] W. Xu, A. Palumbo, J. Xu, Y. Jiang, C.-H. Choi, E.H. Yang, On-demand capture and release of organic droplets using surfactant-doped polypyrrole surfaces, ACS Appl. Mater. Interfaces 9 (2017) 23119–23127, https://doi.org/10.1021/acsami.7b03787.
[59] Y. Jiang, J. Xu, J. Lee, K. Du, E.H. Yang, M.-W. Moon, C.-H. Choi, Nanotexturing of conjugated polymers via one-step maskless oxygen plasma etching for enhanced tunable wettability, Langmuir 33 (2017) 6885–6894, https://doi.org/10.1021/acs.langmuir.7b01593.
[60] K.S. Teh, Y. Takahashi, Z. Yao, Y.-W. Lu, Influence of redox-induced restructuring of polypyrrole on its surface morphology and wettability, Sensors Actuat. A Phys. 155 (2009) 113–119, https://doi.org/10.1016/j.sna.2009.07.006.
[61] L. Bay, T. Jacobsen, S. Skaarup, K. West, Mechanism of actuation in conducting polymers: osmotic expansion, J. Phys. Chem. B 105 (2001) 8492–8497, https://doi.org/10.1021/jp003872w.
[62] P.R. Waghmare, S. Das, S.K. Mitra, Under-water superoleophobic glass: unexplored role of the surfactant-rich solvent, Sci. Rep. 3 (2013) 1862, https://doi.org/10.1038/srep01862.
[63] C. Zhou, J. Feng, J. Cheng, H. Zhang, J. Lin, X. Zeng, P. Pi, Opposite superwetting nickel meshes for on-demand and continuous oil/water separation, Ind. Eng. Chem. Res. 57 (2018) 1059–1070, https://doi.org/10.1021/acs.iecr.7b04517.
[64] N. Li, C. Yu, Y. Si, M. Song, Z. Dong, L. Jiang, Janus gradient meshes for continuous separation and collection of flowing oils under water, ACS Appl. Mater. Interfaces 10 (2018) 7504–7511, https://doi.org/10.1021/acsami.8b00044.
[65] X. Su, H. Li, X. Lai, L. Zhang, X. Liao, J. Wang, Z. Chen, J. He, X. Zeng, Dual-functional superhydrophobic textiles with asymmetric roll-down/pinned states for water droplet transportation and oil-water separation, ACS Appl. Mater. Interfaces 10 (2018) 4213–4221, https://doi.org/10.1021/acsami.7b15909.
[66] X. Chen, Y. He, Y. Fan, Q. Yang, X. Yang, G. Zeng, L. Zhang, A smart engineering material with UV-induced switchable wettability for controllable oil/water separation, J. Chem. Technol. Biotechnol. 93 (2018) 476–488, https://doi.org/10.1002/jctb.5378.
[67] X. Chen, Y. He, Y. Fan, Q. Yang, X. Yang, G. Zeng, Facile preparation of a smart membrane with ammonia-responsive wettability transition for controllable oil/water separation, J. Mater. Sci. 53 (2018) 516–527, https://doi.org/10.1007/s10853-017-1535-2.
[68] C.H. Kung, B. Zahiri, P.K. Sow, W. Mérida, On-demand oil-water separation via low-voltage wettability switching of core-shell structures on copper substrates, Appl. Surf. Sci. 444 (2018) 15–27, https://doi.org/10.1016/j.apsusc.2018.02.238.
[69] Y. Cao, N. Liu, C. Fu, K. Li, L. Tao, L. Feng, Y. Wei, Thermo and pH dual-responsive materials for controllable oil/water separation, ACS Appl. Mater. Interfaces 6 (2014) 2026–2030, https://doi.org/10.1021/am405089m.
[70] A. Rezaee Shirin-Abadi, M. Gorji, S. Rezaee, P.G. Jessop, M.F. Cunningham, CO2 -Switchable-hydrophilicity membrane (CO2 -SHM) triggered by electric potential: faster switching time along with efficient oil/water separation, Chem. Commun. 54 (2018) 8478–8481, https://doi.org/10.1039/C8CC04266G.
[71] T. Yan, X. Chen, T. Zhang, J. Yu, X. Jiang, W. Hu, F. Jiao, A magnetic pH-induced textile fabric with switchable wettability for intelligent oil/water separation, Chem. Eng. J. 347 (2018) 52–63, https://doi.org/10.1016/j.cej.2018.04.021.